

## FOURIER ANALYSIS OF MULTIGRID METHODS ON HEXAGONAL GRIDS\*

GUOHUA ZHOU<sup>†</sup> AND SCOTT R. FULTON<sup>†</sup>

**Abstract.** This paper applies local Fourier analysis to multigrid methods on hexagonal grids. Using oblique coordinates to express the grids and a dual basis for the Fourier modes, the analysis proceeds essentially the same as for rectangular grids. The framework for one- and two-grid analyses is given and then applied to analyze the performance of multigrid methods for the Poisson problem on a hexagonal grid. Numerical results confirm the analysis. Uniform hexagonal grids provide an approximation to spherical geodesic grids; numerical results for the latter show similar performance. While the analysis is similar to that for rectangular grids, the results differ somewhat: full weighting is superior to injection for restriction, Jacobi relaxation performs about as well as Gauss–Seidel relaxation, and underrelaxation is not required for good performance. Also, coarse-fine or four-color ordering (both analogues of red-black ordering on the rectangular grid) improves the performance of Jacobi relaxation, with the latter achieving a smoothing factor of approximately 0.25. An especially simple compact fourth-order discretization works well, and the full multigrid algorithm produces the solution to the level of truncation error in work proportional to the number of unknowns.

**Key words.** multigrid, hexagonal grid, geodesic grid, local Fourier analysis

**AMS subject classifications.** 65N55, 65N06, 65N22

**DOI.** 10.1137/070709566

**1. Introduction.** Discretizations of partial differential equations are often based on structured grids. In two spatial dimensions the most common and natural approach is to use rectangular grids. However, hexagonal grids offer some advantages. In particular, hexagonal grids are more nearly isotropic: each grid cell adjacent to a given cell is located across a cell wall and the same distance away (cf. Figure 2.1 below), in contrast to the rectangular case where neighboring cells share either a wall or a vertex. Consequently, discrete operators may be simpler and truncation errors smaller and more isotropic [6, 7]. Hexagonal grids also play an important role as approximations to the spherical geodesic grids being used increasingly often for numerical modeling in spherical coordinates, e.g., for global climate modeling [4, 5].

Many applications require solving discretized elliptic problems (e.g., the Poisson and modified Helmholtz problems), which can be accomplished efficiently by multigrid methods [3]. These methods combine discretizations on several grids of different mesh size, each covering the whole computational domain; relaxation reduces error components on the scale of each grid, with smooth error components reduced by corrections computed on coarser grids. Introduced in the 1970s by Brandt [1] and others, multigrid methods have become a standard approach on rectangular grids. Heikes and Randall [4] introduced a multigrid method for the Poisson equation on a spherical geodesic grid; this application provided one motivation for the present study.

Local Fourier analysis (LFA) is a key tool for studying multigrid methods, providing estimates of convergence rates which can help guide the design of algorithms and verify that they are implemented correctly. This analysis measures the effect of the multigrid components on discrete Fourier components of the error (or combina-

---

\*Received by the editors November 29, 2007; accepted for publication (in revised form) September 9, 2008; published electronically January 28, 2009.

<http://www.siam.org/journals/sisc/31-2/70956.html>

<sup>†</sup>Department of Mathematics, Clarkson University, Campus Box 5815, Potsdam, NY 13699-5815 (zhoug@clarkson.edu, fulton@clarkson.edu).

tions of components which are coupled). Since LFA ignores boundary conditions and assumes constant-coefficient operators, it does not provide rigorous global bounds on errors. However, in many cases it predicts convergence rates correctly, since reducing nonsmooth error components by relaxation is fundamentally a local task.

The goal of this paper is to use LFA to analyze the performance of multigrid methods on uniform hexagonal grids. While spherical geodesic grids are not perfectly regular and thus not amenable to LFA, they can be closely approximated by uniform hexagonal grids on a plane. Therefore, the results obtained here should be useful in designing multigrid methods for geodesic grids. In particular, Heikes and Randall [4] did not report convergence results for their method; our analysis provides estimates of the theoretical performance of their method and leads to several improvements.

Much of the analysis presented here follows closely that for rectangular grids, once we recognize that hexagonal grids are logically rectangular in oblique coordinates. Therefore, with minor changes we follow the notation and development in [10]. Section 2 introduces notation for operators and Fourier modes on hexagonal grids. Smoothing analysis is presented in section 3 for smoothing operators for which the Fourier modes are eigenfunctions. The corresponding two-grid analysis is given in section 4, including the extension to three-grid analysis. Section 5 considers the case of smoothing operators which couple several Fourier modes and introduces two relaxation schemes which attempt to mimic the properties of red-black ordering on a rectangular grid. Numerical results are given in section 6 which verify the analytical results. Included here are results for the Poisson and modified Helmholtz problems on a hexagonal grid (with various relaxation schemes and grid transfers and using second- and fourth-order discretizations) and sample results from a spherical geodesic grid confirming that the hexagonal-grid analysis gives useful guidance. Section 7 summarizes our conclusions.

**2. Hexagonal grids and operators.** A uniform hexagonal grid is a collection of grid points  $\mathbf{G}_h := \{\mathbf{x}_j^h = (j_1 \mathbf{a}_1 + j_2 \mathbf{a}_2)h : j = (j_1, j_2) \in \mathbb{Z}^2\}$  which are the centers of hexagonal grid cells as shown in Figure 2.1, where

$$\mathbf{a}_1 = \begin{pmatrix} 1 \\ 0 \end{pmatrix}, \quad \mathbf{a}_2 = \begin{pmatrix} 1/2 \\ \sqrt{3}/2 \end{pmatrix}$$

are unit vectors defining the oblique coordinate system and  $h$  is the mesh size (distance between cell centers). This indexing is equivalent to that used in [6]. For LFA the grid  $\mathbf{G}_h$  is considered to be infinite. We assume standard coarsening: the next coarser grid is  $\mathbf{G}_{2h}$  with grid points  $\mathbf{x}_j^{2h} = \mathbf{x}_{2j}^h$  for  $j = (j_1, j_2) \in \mathbb{Z}^2$  as shown in Figure 2.2, and still coarser grids  $\mathbf{G}_{4h}, \mathbf{G}_{8h}, \dots$  are defined similarly.

LFA considers the effects of multigrid processing on the functions  $\varphi_h(\theta, \mathbf{x}) := \exp(i\theta \cdot \mathbf{x}/h)$ , where  $\theta \in \mathbb{R}^2$  is the Fourier wave number relative to  $\mathbf{G}_h$ . We will use the term “mode” to refer to either the function  $\varphi_h(\theta, \mathbf{x})$  or its associated wave number  $\theta$ . On the hexagonal grid it is convenient to write  $\theta = \theta_1 \mathbf{b}_1 + \theta_2 \mathbf{b}_2$ , where  $\{\mathbf{b}_1, \mathbf{b}_2\}$  is the dual basis corresponding to  $\{\mathbf{a}_1, \mathbf{a}_2\}$ , i.e.,

$$\mathbf{b}_1 = \begin{pmatrix} 1 \\ -1/\sqrt{3} \end{pmatrix}, \quad \mathbf{b}_2 = \begin{pmatrix} 0 \\ 2/\sqrt{3} \end{pmatrix}$$

satisfying  $\mathbf{a}_i \cdot \mathbf{b}_j = \delta_{ij}$ . Then on grid  $\mathbf{G}_h$  we have  $\varphi_h(\theta, \mathbf{x}_j^h) = \exp[i(j_1 \theta_1 + j_2 \theta_2)]$  for  $j \in \mathbb{Z}^2$ . Since  $\varphi_h(\theta, \mathbf{x}) = \varphi_h(\theta', \mathbf{x})$  for all  $\mathbf{x} \in \mathbf{G}_h$  if and only if  $\theta_1 = \theta'_1 \bmod 2\pi$  and  $\theta_2 = \theta'_2 \bmod 2\pi$ , we see that the Fourier modes  $\varphi_h(\theta, \mathbf{x})$  are distinguishable on the

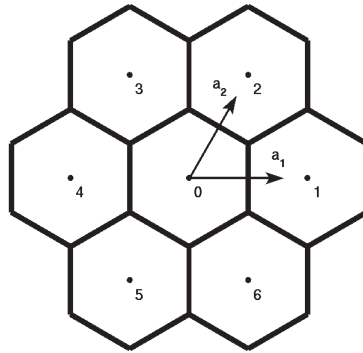


FIG. 2.1. A uniform hexagonal grid  $\mathbf{G}_h$ . The cell centers are grid points (indexed 0 through 6 as in (2.2)), and the unit vectors  $\mathbf{a}_1$  and  $\mathbf{a}_2$  define the oblique coordinate system.

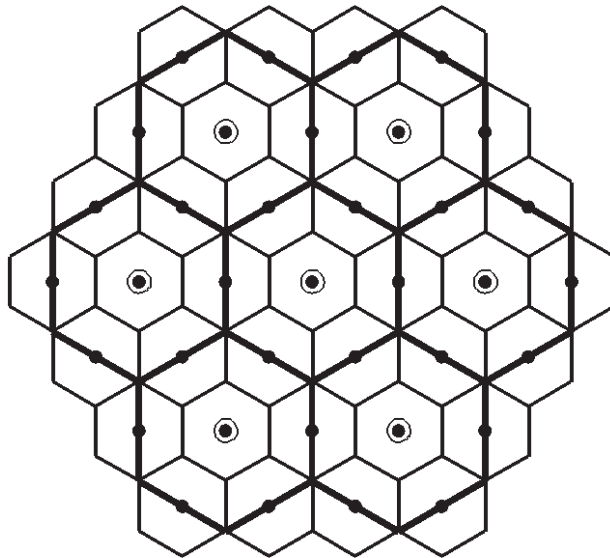


FIG. 2.2. Relation between fine grid (dots and thin lines) and coarse grid (circles and thick lines).

grid  $\mathbf{G}_h$  only for  $\theta \in \Theta := [-\pi, \pi)^2$ , which we refer to as the modes *visible* on the grid. Note that for points on grid  $\mathbf{G}_{2h}$ ,  $\varphi_h(\theta, \mathbf{x}_{2j}^h) = \varphi_{2h}(2\theta, \mathbf{x}_j^{2h})$ ; i.e., a mode with wave number  $\theta$  relative to  $\mathbf{G}_h$  has wave number  $2\theta$  relative to  $\mathbf{G}_{2h}$ . Thus, we can partition the set  $\Theta$  of modes visible on a grid  $\mathbf{G}_h$  into the set  $\Theta_{\text{low}} := [-\pi/2, \pi/2)^2$  of *low modes*, which are visible on the next coarser grid  $\mathbf{G}_{2h}$ , and the set  $\Theta_{\text{high}} := \Theta \setminus \Theta_{\text{low}}$  of *high modes*, which are not.

The discrete operators considered here are assumed to be linear with constant coefficients. Such an operator  $L_h$  corresponds to a *stencil*  $[s_k]_h$  indexed by  $k = (k_1, k_2) \in \mathbb{Z}^2$ , which means that for any grid function  $u_h$  defined on  $\mathbf{G}_h$ ,

$$(2.1) \quad L_h u_h(\mathbf{x}_j^h) = \sum_{k \in K} s_k u_h(\mathbf{x}_{j+k}^h), \quad \mathbf{x}_j^h \in \mathbf{G}_h,$$

where the coefficients  $s_k$  may depend on  $h$  (but not on  $j$ ) and  $K \subset \mathbb{Z}^2$  is a finite index set. For such operators the following lemma holds.

LEMMA 2.1. For any discrete operator  $L_h$  on  $\mathbf{G}_h$  described by a difference stencil of the form (2.1), all Fourier modes  $\varphi_h(\theta, \mathbf{x})$  are eigenfunctions, with

$$L_h \varphi_h(\theta, \mathbf{x}) = \tilde{L}_h(\theta) \varphi_h(\theta, \mathbf{x}), \quad \mathbf{x} \in \mathbf{G}_h,$$

where the eigenvalue  $\tilde{L}_h(\theta) := \sum_{k \in K} s_k e^{i(k_1 \theta_1 + k_2 \theta_2)}$  is called the symbol of  $L_h$ .

For example, the (negative) Laplacian operator  $-\nabla^2$  can be discretized using seven points as

$$(2.2) \quad L_h u_0 = \frac{2}{3h^2} \left( 6u_0 - \sum_{i=1}^6 u_i \right),$$

where for convenience we have used different indexing: the subscripts 0 and 1–6 denote the central point and its six nearest neighbors, respectively, as shown in Figure 2.1. Expressing these points in the oblique coordinate gives the stencil

$$\frac{2}{3h^2} \begin{bmatrix} -1 & -1 & 0 \\ -1 & 6 & -1 \\ 0 & -1 & -1 \end{bmatrix}_h$$

with corresponding symbol

$$(2.3) \quad \tilde{L}_h(\theta) = \frac{4}{3h^2} [3 - \cos(\theta_1) - \cos(\theta_2) - \cos(\theta_2 - \theta_1)].$$

It can be shown that this discretization is second-order accurate.

**3. Smoothing analysis.** The performance of a multigrid method depends in large part on the effectiveness of the relaxation scheme which smoothes the error on each grid. In this section we analyze relaxation schemes for which the Fourier modes are eigenfunctions of the corresponding smoothing operators. If we express the hexagonal grid using oblique coordinates and Fourier modes using the dual basis, the analysis proceeds essentially the same as for rectangular grids (cf. [10, section 4.3]).

Consider a discretized partial differential equation  $L_h u_h = f_h$ , and assume that a relaxation scheme can be written via an operator splitting  $L_h = L_h^+ + L_h^-$  (where  $L_h^+$  is invertible) as

$$(3.1) \quad L_h^+ \bar{u}_h + L_h^- \tilde{u}_h = f_h,$$

where  $\tilde{u}_h$  and  $\bar{u}_h$  are the old and new approximations to the true discrete solution  $u_h$ , respectively. Subtracting (3.1) from the discrete equation  $L_h u_h = f_h$  shows that the old and new errors  $\tilde{v}_h = u_h - \tilde{u}_h$  and  $\bar{v}_h = u_h - \bar{u}_h$  satisfy

$$\bar{v}_h = S_h \tilde{v}_h,$$

where  $S_h := -(L_h^+)^{-1} L_h^-$  is the resulting *smoothing operator*. Applying  $L_h^+$ ,  $L_h^-$ , and  $S_h$  to the Fourier modes  $\varphi_h(\theta, \mathbf{x})$ , we have the following lemma.

LEMMA 3.1. For any relaxation scheme of the form (3.1), all Fourier modes  $\varphi_h(\theta, \mathbf{x})$  for which  $\tilde{L}_h^+(\theta) \neq 0$  are eigenfunctions of the smoothing operator  $S_h$ , with

$$S_h \varphi_h(\theta, \mathbf{x}) = \tilde{S}_h(\theta) \varphi_h(\theta, \mathbf{x}), \quad \mathbf{x} \in \mathbf{G}_h,$$

where the symbol of the smoothing operator, given by  $\tilde{S}_h(\theta) := -\tilde{L}_h^-(\theta)/\tilde{L}_h^+(\theta)$ , is called the amplification factor.

The effectiveness of relaxation as a smoother is then measured by the *multigrid smoothing factor*

$$(3.2) \quad \mu_1(S_h) := \sup \left\{ \left| \tilde{S}_h(\theta) \right| : \theta \in \Theta_{\text{high}} \right\},$$

which quantifies how well relaxation reduces the high-mode error components. Assuming that the low-mode error components are eliminated by corrections computed on the coarse grids, the smoothing factor gives an estimate of the overall efficiency of the multigrid method.

For example, consider the Poisson equation  $-\nabla^2 u = f$  with the discretization (2.2). Weighted Jacobi (WJ) relaxation (as used in [4]) can be formulated as

$$\bar{u}_0 = (1 - \omega)\bar{u}_0 + \frac{\omega}{6} \left( \frac{3h^2}{2} f_0 + \sum_{i=1}^6 \bar{u}_i \right),$$

where  $\omega$  is a relaxation parameter to allow for under- or overrelaxation. The corresponding smoothing operator is

$$(S_h^J(\omega)v_h)_0 = (1 - \omega)v_0 + \frac{\omega}{6} \sum_{i=1}^6 v_i$$

with symbol

$$(3.3) \quad \tilde{S}_h^J(\theta, \omega) = 1 - \frac{2\omega}{3} \left[ \sin^2 \left( \frac{\theta_1}{2} \right) + \sin^2 \left( \frac{\theta_2}{2} \right) + \sin^2 \left( \frac{\theta_1 - \theta_2}{2} \right) \right].$$

For smoothing  $\omega$  must be positive, and it can be shown that the smoothing factor is

$$\mu_1(S_h^J(\omega)) = \max \left\{ 1 - \omega \left( 1 - \frac{\sqrt{2}}{3} \right), \frac{3\omega}{2} - 1 \right\},$$

with the first and second values corresponding to extrema on the inner boundary and interior of the high-mode region  $\Theta_{\text{high}}$ , respectively. The optimum smoothing is obtained with  $\omega = 12/(15 - 2\sqrt{2}) \approx 0.9859$ , for which the smoothing factor is approximately 0.4789. Also, the simpler unweighted Jacobi scheme (i.e., with  $\omega = 1$ ) gives the smoothing factor 0.5, which is nearly as good; this differs from the situation on a rectangular grid in which underrelaxation ( $\omega < 1$ ) is required.

Similarly, for (weighted) Gauss–Seidel (GS) relaxation—with lexicographic ordering in the oblique coordinate—we obtain the symbol

$$(3.4) \quad \tilde{S}_h^G(\theta, \omega) = \frac{6(1 - \omega) + \omega [e^{i\theta_1} + e^{i\theta_2} + e^{i(\theta_2 - \theta_1)}]}{6 - \omega [e^{-i\theta_1} + e^{-i\theta_2} + e^{-i(\theta_2 - \theta_1)}]},$$

where  $\omega$  is again the relaxation parameter. For  $0 < \omega < 2$  the maximum in (3.2) is obtained on the inner boundary of the high-mode region  $\Theta_{\text{high}}$ . The resulting smoothing factor for unweighted Gauss–Seidel ( $\omega = 1$ ) is approximately 0.5399, only marginally higher than the optimum value 0.5396 obtained at  $\omega = 1.02$ . This result is slightly *worse* than for Jacobi relaxation; this is the opposite of the situation for the standard five-point discretization on the rectangular grid but similar to that for some nine-point discretizations [13].

**4. Two-grid analysis.** Two-grid analysis improves upon smoothing analysis by including the effects of grid transfers in addition to the smoothing by relaxation. In a two-grid cycle, the coarse-grid correction is computed by calculating the residual on the fine grid  $\mathbf{G}_h$ , transferring it to the coarse grid  $\mathbf{G}_{2h}$ , solving the residual equation there, and transferring the resulting correction back to the fine grid. The effect on the fine-grid error is represented by the *coarse-grid correction operator*

$$(4.1) \quad K_h^{2h} := I_h - I_{2h}^h (L_{2h})^{-1} I_h^{2h} L_h,$$

where  $I_h^{2h}$  is the restriction operator,  $I_{2h}^h$  is the prolongation (interpolation) operator,  $I_h$  is the identity operator on grid  $\mathbf{G}_h$ , and we have assumed that the coarse-grid operator  $L_{2h}$  is invertible. A two-grid cycle consisting of  $\nu_1$  and  $\nu_2$  relaxation sweeps on the fine grid before and after the coarse-grid correction, respectively, can be represented by the *two-grid operator*

$$(4.2) \quad M_h^{2h} := S_h^{\nu_2} K_h^{2h} S_h^{\nu_1}.$$

This two-grid cycle is an approximation to a multigrid  $V(\nu_1, \nu_2)$  cycle, which is obtained by recursively solving the coarse-grid problem by the same approach (i.e.,  $\nu_1$  and  $\nu_2$  relaxation sweeps before and after a coarse-grid correction).

Two-grid analysis measures the effect of  $M_h^{2h}$  on the fine-grid errors; it is more complicated than smoothing analysis since the grid transfers couple the high and low modes. Again, if we express the hexagonal grid using the oblique coordinate and Fourier modes using the dual basis, the analysis proceeds essentially the same as for rectangular grids (cf. [10, section 4.4]). The key to the analysis is the use of spaces of harmonics which are invariant under the operators. For any  $\theta = (\theta_1, \theta_2) \in \Theta$  let

$$\theta^{(0)} := (\theta_1, \theta_2), \quad \theta^{(1)} := (\bar{\theta}_1, \theta_2), \quad \theta^{(2)} := (\theta_1, \bar{\theta}_2), \quad \theta^{(3)} := (\bar{\theta}_1, \bar{\theta}_2),$$

where

$$\bar{\theta}_i := \begin{cases} \theta_i + \pi & \text{if } \theta_i < 0, \\ \theta_i - \pi & \text{if } \theta_i \geq 0. \end{cases}$$

Precisely one of these four modes is a low mode; while the following development holds for any  $\theta \in \Theta$ , we can for concreteness assume that  $\theta^{(0)} = \theta \in \Theta_{\text{low}}$  as in Figure 4.1. These four modes coincide on the coarse-grid points  $\mathbf{x}_j^{2h} = \mathbf{x}_{2j}^h$ , i.e.,

$$\varphi_h(\theta^{(\ell)}, \mathbf{x}_{2j}^h) = \varphi_h(\theta, \mathbf{x}_{2j}^h) = \varphi_{2h}(2\theta, \mathbf{x}_j^{2h}), \quad \ell = 0, 1, 2, 3.$$

Since they are linearly independent, they form a basis for the *space of harmonics*  $\mathbf{E}_h^\theta := \text{span} \{ \varphi_h(\theta^{(\ell)}, \cdot) : \ell = 0, 1, 2, 3 \}$ . Any grid function  $\psi_h \in \mathbf{E}_h^\theta$  can be represented in the form

$$(4.3) \quad \psi_h(\mathbf{x}) = \sum_{\ell=0}^3 A^{(\ell)} \varphi_h(\theta^{(\ell)}, \mathbf{x}), \quad \mathbf{x} \in \mathbf{G}_h.$$

Since  $e^{i\bar{\theta}_\ell} = -e^{i\theta_\ell}$ , we can also write

$$(4.4) \quad \psi_h(\mathbf{x}) = \Psi_h(\mathbf{x}) \varphi_h(\theta, \mathbf{x}), \quad \mathbf{x} \in \mathbf{G}_h,$$

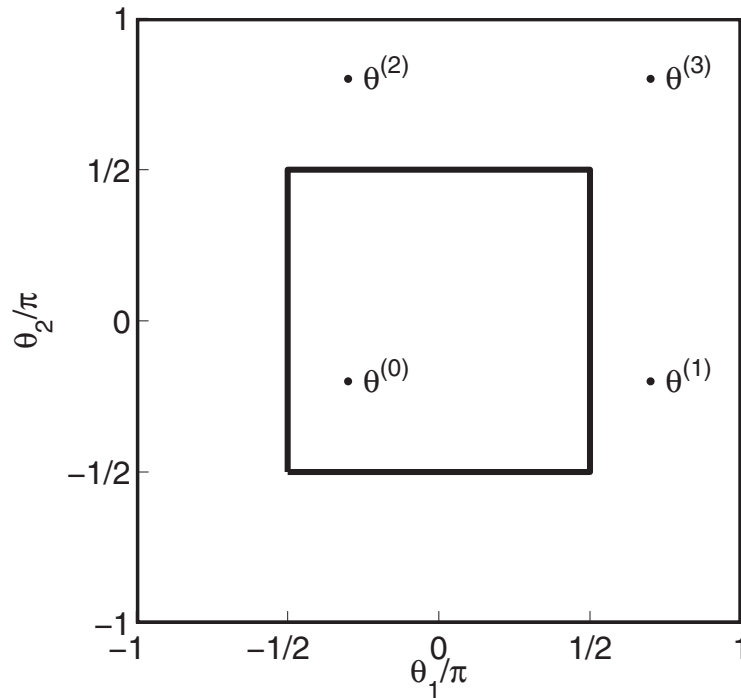


FIG. 4.1. Four modes defining the space  $\mathbf{E}_h^\theta$  of harmonics.

where  $\Psi_h$  has the *four-color* pattern

$$(4.5) \quad \Psi_h(\mathbf{x}_j^h) = \begin{cases} \Psi^{(0)} & \text{if } j_1 \text{ even and } j_2 \text{ even,} \\ \Psi^{(1)} & \text{if } j_1 \text{ odd and } j_2 \text{ even,} \\ \Psi^{(2)} & \text{if } j_1 \text{ even and } j_2 \text{ odd,} \\ \Psi^{(3)} & \text{if } j_1 \text{ odd and } j_2 \text{ odd,} \end{cases}$$

with values  $\Psi^{(\ell)}$  given in terms of coefficients  $A^{(\ell)}$  by

$$(4.6) \quad \begin{pmatrix} \Psi^{(0)} \\ \Psi^{(1)} \\ \Psi^{(2)} \\ \Psi^{(3)} \end{pmatrix} = \begin{pmatrix} 1 & 1 & 1 & 1 \\ 1 & -1 & 1 & -1 \\ 1 & 1 & -1 & -1 \\ 1 & -1 & -1 & 1 \end{pmatrix} \begin{pmatrix} A^{(0)} \\ A^{(1)} \\ A^{(2)} \\ A^{(3)} \end{pmatrix}.$$

Since the matrix in (4.6) is invertible, the two representations (4.3) and (4.4) of  $\psi_h \in \mathbf{E}_h^\theta$  are complementary.

Under appropriate assumptions, the space  $\mathbf{E}_h^\theta$  is invariant under the operators  $K_h^{2h}$  and  $M_h^{2h}$ , which, therefore, may be represented by  $4 \times 4$  matrices  $\widehat{K}_h^{2h}(\theta)$  and  $\widehat{M}_h^{2h}(\theta)$ , respectively. This means that if  $\psi^h \in \mathbf{E}_h^\theta$ , then  $M_h^{2h}\psi_h \in \mathbf{E}_h^\theta$  as well, with coefficients in the expansion form (4.3) given by the matrix  $\widehat{M}_h^{2h}(\theta)$  times the vector of coefficients of  $\psi_h$ . This result is established—and the details of  $\widehat{K}_h^{2h}(\theta)$  and  $\widehat{M}_h^{2h}(\theta)$  are obtained—by examining the effects of the discrete operators, smoothing, and grid transfers as follows (the proofs are essentially the same as for rectangular grids and hence are omitted).

*Discrete operators.* Given that the fine-grid operator  $L_h$  is represented by a stencil  $[s_k(h)]_h$ , it is a linear operator on  $\mathbf{E}_h^\theta$ . From Lemma 2.1 the matrix representation is

$$\widehat{L}_h(\theta) = \text{diag} \left( \widetilde{L}_h \left( \theta^{(0)} \right), \widetilde{L}_h \left( \theta^{(1)} \right), \widetilde{L}_h \left( \theta^{(2)} \right), \widetilde{L}_h \left( \theta^{(3)} \right) \right).$$

Likewise, the coarse-grid operator  $L_{2h}$ , given by stencil  $[s_k(2h)]_{2h}$ , acting on  $\varphi_{2h}(2\theta, \mathbf{x})$  produces

$$(4.7) \quad L_{2h}\varphi_{2h}(2\theta, \mathbf{x}) = \widetilde{L}_{2h}(2\theta)\varphi_{2h}(2\theta, \mathbf{x}), \quad \mathbf{x} \in \mathbf{G}_{2h}.$$

Note that while the discrete operator should be invertible on a finite grid (with boundary conditions) often it is not on an infinite grid (e.g., the Laplacian of a nonzero constant is zero). The two-grid analysis assumes the coarse-grid equation is solved exactly, so we omit the null space of  $\widetilde{L}_{2h}$ , i.e.,

$$\Theta_0 = \left\{ \theta \in \Theta_{\text{low}} : \widetilde{L}_{2h}(2\theta) = 0 \right\}.$$

For example, for the discrete Laplacian (2.2) with symbol given by (2.3), the null space  $\Theta_0$  contains only the single mode  $\theta = (0, 0)$ .

*Smoothing.* If the space  $\mathbf{E}_h^\theta$  is invariant under the smoothing operator  $S_h$ , then  $S_h$  can be represented by a  $4 \times 4$  matrix  $\widehat{S}_h(\theta)$ . In the special case where all Fourier modes are eigenfunctions of  $S_h$  as in Lemma 3.1, this matrix takes the simple form

$$\widehat{S}_h(\theta) = \text{diag} \left( \widetilde{S}_h \left( \theta^{(0)} \right), \widetilde{S}_h \left( \theta^{(1)} \right), \widetilde{S}_h \left( \theta^{(2)} \right), \widetilde{S}_h \left( \theta^{(3)} \right) \right).$$

For example, with WJ or GS relaxation the matrix takes this form using (3.3) or (3.4), respectively. If the Fourier modes are not eigenfunctions of  $S_h$ , then the matrix  $\widehat{S}_h(\theta)$  is not diagonal and must be computed directly; examples are given in section 5.

*Restriction.* We assume that the restriction operator  $I_h^{2h}$  is represented by a stencil  $[\hat{t}_k]_h^{2h}$  indexed by  $k$  in some finite index set  $K_R \subset \mathbb{Z}^2$ . Here  $\hat{t}_k$  is the weight of the contribution to the coarse-grid value at  $\mathbf{x}_j^{2h}$  from the fine-grid value at  $\mathbf{x}_{2j+k}^h$ , i.e.,

$$(4.8) \quad (I_h^{2h}\psi_h) (\mathbf{x}_j^{2h}) = \sum_{k \in K_R} \hat{t}_k \psi_h (\mathbf{x}_{2j+k}^h).$$

Such a restriction satisfies the following lemma.

LEMMA 4.1. *If  $\psi_h \in \mathbf{E}_h^\theta$  with coefficients  $A^{(\ell)}$  in the representation (4.3), then the restriction (4.8) produces  $\psi_{2h} = I_h^{2h}\psi_h$  satisfying  $\psi_{2h}(\mathbf{x}) = A_{2h}\varphi_{2h}(2\theta, \mathbf{x})$  for  $\mathbf{x} \in \mathbf{G}_{2h}$  with*

$$(4.9) \quad A_{2h} = \left( \widetilde{I}_h^{2h} \left( \theta^{(0)} \right), \widetilde{I}_h^{2h} \left( \theta^{(1)} \right), \widetilde{I}_h^{2h} \left( \theta^{(2)} \right), \widetilde{I}_h^{2h} \left( \theta^{(3)} \right) \right) \begin{pmatrix} A^{(0)} \\ A^{(1)} \\ A^{(2)} \\ A^{(3)} \end{pmatrix},$$

where  $\widetilde{I}_h^{2h}(\theta) := \sum_{k \in K_R} \hat{t}_k e^{ik \cdot \theta}$  is the symbol of the restriction operator.

Thus, the restriction  $I_h^{2h}$  is represented by the  $1 \times 4$  matrix on the right side of (4.9), which we denote by  $\widetilde{I}_h^{2h}(\theta)$ . Perhaps the most natural restriction is *full weighting*, which on the hexagonal grid has the stencil

$$\frac{1}{8} \begin{bmatrix} 1 & 1 & 0 \\ 1 & 2 & 1 \\ 0 & 1 & 1 \end{bmatrix}_h^{2h}$$

and corresponding symbol  $\tilde{I}_h^{2h}(\theta) = \frac{1}{4}[1 + \cos(\theta_1) + \cos(\theta_2) + \cos(\theta_2 - \theta_1)]$ . We will also consider *injection*, with stencil  $[1]_h^{2h}$  and corresponding symbol  $\tilde{I}_h^{2h}(\theta) = 1$ .

*Prolongation.* We likewise assume that the prolongation operator  $I_{2h}^h$  is represented by a stencil  $]t_k[_{2h}^h$  indexed by  $k$  in some finite index set  $K_P \subset \mathbb{Z}^2$ . Here  $t_k$  is the weight of the contribution from the coarse-grid value at  $\mathbf{x}_j^{2h}$  to the fine-grid value at  $\mathbf{x}_{2j+k}^h$ . This can be written explicitly in the form

$$(4.10) \quad (I_{2h}^h \psi_{2h})(\mathbf{x}_{2j+k}^h) = \sum_{k'} t_{2k'+k} \psi_{2h}(\mathbf{x}_{j-k'}^{2h}),$$

where the sum is over all  $k' \in \mathbb{Z}^2$  for which  $2k' + k \in K_P$ . Using the four-color form (4.4) it can be shown that such a prolongation satisfies the following lemma.

LEMMA 4.2. *If  $\psi_{2h}(\mathbf{x}) = A_{2h} \varphi_{2h}(2\theta, \mathbf{x})$  for  $\mathbf{x} \in \mathbf{G}_{2h}$ , then the prolongation (4.10) produces  $\psi_h = I_{2h}^h \psi_{2h} \in \mathbf{E}_h^\theta$ , and its coefficients  $A^{(\ell)}$  in the representation (4.3) satisfy*

$$(4.11) \quad \begin{pmatrix} A^{(0)} \\ A^{(1)} \\ A^{(2)} \\ A^{(3)} \end{pmatrix} = \begin{pmatrix} \tilde{I}_{2h}^h(\theta^{(0)}) \\ \tilde{I}_{2h}^h(\theta^{(1)}) \\ \tilde{I}_{2h}^h(\theta^{(2)}) \\ \tilde{I}_{2h}^h(\theta^{(3)}) \end{pmatrix} A_{2h},$$

where  $\tilde{I}_{2h}^h(\theta) := \frac{1}{4} \sum_{k \in K_P} t_k e^{-ik \cdot \theta}$  is the symbol of the prolongation operator.

Thus, the prolongation  $I_{2h}^h$  is represented by the  $4 \times 1$  matrix on the right side of (4.11), which we denote by  $\hat{I}_{2h}^h(\theta)$ . The natural prolongation on a hexagonal grid is “bilinear” interpolation (more precisely, linear interpolation between nearest neighbors), with stencil

$$\frac{1}{2} \begin{bmatrix} 1 & 1 & 0 \\ 1 & 2 & 1 \\ 0 & 1 & 1 \end{bmatrix}_{2h}^h$$

and corresponding symbol  $\tilde{I}_{2h}^h(\theta) = \frac{1}{4}[1 + \cos(\theta_1) + \cos(\theta_2) + \cos(\theta_2 - \theta_1)]$ . Comparing Lemmas 4.1 and 4.2 we see that if  $\hat{t}_k = t_k/4$ , then the restriction and prolongation operators are adjoints of each other; in particular, this is true for full weighting and bilinear interpolation.

Putting the above pieces together establishes the following theorem.

THEOREM 4.3. *Suppose that the discrete operators  $L_h$  and  $L_{2h}$  and grid transfers  $I_h^{2h}$  and  $I_{2h}^h$  are represented by stencils. Then for any  $\theta \in \Theta_{low} \setminus \Theta_0$  the space  $\mathbf{E}_h^\theta$  is invariant under the coarse-grid correction operator  $K_h^{2h}$ , which is represented by the  $4 \times 4$  matrix*

$$\hat{K}_h^{2h}(\theta) = \hat{I}_h - \hat{I}_{2h}^h(\theta) \left( \tilde{L}_{2h}(2\theta) \right)^{-1} \hat{I}_h^{2h}(\theta) \hat{L}_h(\theta),$$

where  $\hat{I}_h$  is the  $4 \times 4$  identity matrix. Furthermore, if  $\mathbf{E}_h^\theta$  is invariant under the smoothing operator  $S_h$ , then it is also invariant under the two-grid operator  $M_h^{2h}$ , which is represented by the  $4 \times 4$  matrix

$$(4.12) \quad \hat{M}_h^{2h}(\theta) = \hat{S}_h(\theta)^{\nu_2} \hat{K}_h^{2h}(\theta) \hat{S}_h(\theta)^{\nu_1}.$$

The effectiveness of the two-grid cycle is then measured by the *asymptotic convergence factor*

$$(4.13) \quad \rho_2 (M_h^{2h}) := \sup \left\{ \rho \left( \widehat{M}_h^{2h}(\theta) \right) : \theta \in \Theta_{\text{low}} \setminus \Theta_0 \right\},$$

where  $\rho(\cdot)$  denotes the spectral radius. For comparison with the (one-grid) smoothing analysis it is convenient to calculate the corresponding *two-grid smoothing factor*

$$(4.14) \quad \mu_2 := \left[ \rho_2 (M_h^{2h}) \right]^{1/(\nu_1 + \nu_2)},$$

which estimates the convergence per fine-grid relaxation sweep. Values of  $\mu_2$  will be compared with the numerical results in section 6.

Finally, two-grid analysis can be extended recursively to three (or more) grids as described in [11, 12]. In some cases this analysis may be needed, e.g., when using different discretizations on different grids or different numbers of presmoothing and postsmoothing sweeps. Although we do not consider such cases here, the three-grid analysis is a simple extension of the two-grid analysis, so we mention it here for completeness. A three-grid cycle with  $\gamma$  coarse-grid corrections per level (e.g.,  $\gamma = 1$  for a V-cycle,  $\gamma = 2$  for a W-cycle, etc.) is represented by the three-grid operator

$$M_h^{4h} = S_h^{\nu_2} \left[ I_h - I_{2h}^h (I_{2h} - (M_{2h}^{4h})^\gamma) (L_{2h})^{-1} I_h^{2h} L_h \right] S_h^{\nu_1},$$

where  $M_{2h}^{4h}$  is defined by (4.2) with  $h$  replaced by  $2h$ , i.e.,

$$M_{2h}^{4h} := S_{2h}^{\nu_2} \left[ I_{2h} - I_{4h}^{2h} (L_{4h})^{-1} I_{2h}^{4h} L_{2h} \right] S_{2h}^{\nu_1}.$$

Thus, the three-grid operator  $M_h^{4h}$  is obtained by replacing  $(L_{2h})^{-1}$  in (4.1)–(4.2) by

$$(L_{2h}^{4h})^{-1} = \left( I_{2h} - (M_{2h}^{4h})^\gamma \right) (L_{2h})^{-1}.$$

Since each of the four harmonics for the grid  $\mathbf{G}_{2h}$  is coupled to four harmonics on grid  $\mathbf{G}_h$ , the operator  $M_h^{4h}$  couples harmonics in a 16-dimensional space and thus is represented by a  $16 \times 16$  matrix  $\widehat{M}_h^{4h}$ . The details are the same as for rectangular grids (see [12]) and thus will not be presented here. The effectiveness of the three-grid cycle is then measured by the *asymptotic convergence factor*

$$(4.15) \quad \rho_3 (M_h^{4h}) := \sup \left\{ \rho \left( \widehat{M}_h^{4h}(\theta) \right) : \theta \in \Theta_{\text{low}} \setminus \Theta_0 \right\},$$

where in this context  $\Theta_{\text{low}} = [-\pi/4, \pi/4]^2$  and  $\Theta_0$  is the null space of  $\widetilde{L}_{4h}$ . The corresponding *three-grid smoothing factor*

$$(4.16) \quad \mu_3 := \left[ \rho_3 (M_h^{4h}) \right]^{1/(\nu_1 + \nu_2)}$$

estimates the convergence per fine-grid relaxation sweep.

**5. Smoothing analysis revisited.** The smoothing analysis in section 3 assumes that all Fourier modes  $\varphi_h(\theta, \cdot)$  are eigenfunctions of the smoothing operator  $S_h$ . However, some smoothers do not satisfy this assumption but instead couple the high and low modes. For such smoothers the notation of the previous section allows us to extend the (one-grid) smoothing analysis, exactly as in the case of rectangular grids (cf. [10, section 4.5]). Specifically, if the spaces  $\mathbf{E}_h^\theta$  are invariant under the

smoothing operator  $S_h$ , we can generalize the definition (3.2) of the smoothing factor to read

$$\mu_1(S_h, \nu) := \sup \left\{ \left[ \rho \left( \widehat{Q}_h^{2h} \widehat{S}_h(\theta)^\nu \right) \right]^{1/\nu} : \theta \in \Theta_{\text{low}} \right\},$$

where the diagonal matrix  $\widehat{Q}_h^{2h}$  represents the perfect coarse-grid correction, with  $\theta = \theta^{(0)} \in \Theta_{\text{low}}$ ,  $\widehat{Q}_h^{2h} = \text{diag}(0, 1, 1, 1)$ .

An important example of such a smoother on a rectangular grid is Gauss–Seidel relaxation with red-black ordering (RB), which achieves superior performance. While this has no direct analogue on the hexagonal grid, two orderings for weighted Jacobi relaxation retain some features of RB relaxation and thus merit investigation.

**5.1. Coarse-fine ordering.** On a rectangular grid, RB relaxation has the property that only one of the two partial sweeps changes values at points corresponding to the coarse grid. This can be achieved on the hexagonal grid by weighted Jacobi relaxation with *coarse-fine* (CF) ordering, which is often used in algebraic multigrid methods [2, 8]. One CF sweep consists of two partial sweeps of (weighted) Jacobi relaxation at points  $\mathbf{x}_j^h$  on grid  $\mathbf{G}_h$ :

- coarse sweep:*  $j_1$  even and  $j_2$  even,
- fine sweep:* remaining points  $x_j^h$ .

The smoothing operator for a complete CF sweep is thus  $S_h^{CF} = S_h^F S_h^C$ , where  $S_h^C$  and  $S_h^F$  are the operators representing the coarse and fine sweeps, respectively. When applied to a Fourier mode  $\varphi_h(\theta, \cdot)$ , each of these partial sweeps produces a result with the four-color pattern (4.4)–(4.5), so  $\mathbf{E}_h^\theta$  is invariant under  $S_h^{CF}$ . Specifically, for each Fourier mode the coarse sweep produces  $S_h^C \varphi_h(\theta, \mathbf{x}) = \Psi_h^C(\mathbf{x}) \varphi_h(\theta, \mathbf{x})$  for  $\mathbf{x} \in \mathbf{G}_h$ , where

$$\Psi_h^C(\mathbf{x}_j^h) = \begin{cases} \widetilde{S}_h^J(\theta, \omega) & \text{if } j_1 \text{ even and } j_2 \text{ even,} \\ 1 & \text{otherwise,} \end{cases}$$

with  $\widetilde{S}_h^J$  the symbol of the smoothing operator for weighted Jacobi relaxation for the Laplacian, given by (3.3). Using (4.6) to express this result in terms of the basis of  $\mathbf{E}_h^\theta$  and applying this result to the four basis modes  $\theta^{(\ell)}$ ,  $\ell = 0, 1, 2, 3$ , leads to the matrix representation

$$(5.1) \quad \widehat{S}_h^C(\theta) = \begin{pmatrix} a_0 & b_1 & b_2 & b_3 \\ b_0 & a_1 & b_2 & b_3 \\ b_0 & b_1 & a_2 & b_3 \\ b_0 & b_1 & b_2 & a_3 \end{pmatrix},$$

where  $a_\ell := \frac{1}{4}(\widetilde{S}_h^J(\theta^{(\ell)}, \omega) + 3)$  and  $b_\ell := \frac{1}{4}(\widetilde{S}_h^J(\theta^{(\ell)}, \omega) - 1)$ . Similarly, for the fine sweep we obtain

$$\widehat{S}_h^F(\theta) = \begin{pmatrix} c_0 & d_1 & d_2 & d_3 \\ d_0 & c_1 & d_2 & d_3 \\ d_0 & d_1 & c_2 & d_3 \\ d_0 & d_1 & d_2 & c_3 \end{pmatrix},$$

where  $c_\ell := \frac{1}{4}(1 + 3\widetilde{S}_h^J(\theta^{(\ell)}, \omega))$  and  $d_\ell := \frac{1}{4}(1 - \widetilde{S}_h^J(\theta^{(\ell)}, \omega))$ . Note that  $\widetilde{S}_h^J$  depends on the relaxation parameter  $\omega$ , which may be chosen differently for the coarse and fine sweeps.

**5.2. Four-color ordering.** For the Laplacian operator on a rectangular grid, RB relaxation also has the property that each partial sweep operates on points which are decoupled. This can be achieved on the hexagonal grid by weighted Jacobi relaxation with *four-color* (4C) ordering (suggested by Ross Heikes). One 4C sweep consists of four partial sweeps of (weighted) Jacobi relaxation at points  $\mathbf{x}_j^h$  on grid  $\mathbf{G}_h$ :

- sweep 1:* points  $x_j^h$  with  $j_1$  even and  $j_2$  even,
- sweep 2:* points  $x_j^h$  with  $j_1$  odd and  $j_2$  even,
- sweep 3:* points  $x_j^h$  with  $j_1$  even and  $j_2$  odd,
- sweep 4:* points  $x_j^h$  with  $j_1$  odd and  $j_2$  odd.

The smoothing operator for the full sweep is  $S_h^{4C} = S_h^{(4)} S_h^{(3)} S_h^{(2)} S_h^{(1)}$ , where  $S_h^{(\ell)}$  is the operator for sweep  $\ell = 1, 2, 3, 4$ . Sweep 1 is the same as the coarse sweep of CF relaxation, so it is represented by the matrix  $\widehat{S}_h^{(1)} = \widehat{S}_h^C$  given by (5.1). The remaining sweeps are represented by the corresponding matrices

$$\widehat{S}_h^{(2)}(\theta) = \begin{pmatrix} a_0 & -b_1 & b_2 & -b_3 \\ -b_0 & a_1 & -b_2 & b_3 \\ b_0 & -b_1 & a_2 & -b_3 \\ -b_0 & b_1 & -b_2 & a_3 \end{pmatrix}, \quad \widehat{S}_h^{(3)}(\theta) = \begin{pmatrix} a_0 & b_1 & -b_2 & -b_3 \\ b_0 & a_1 & -b_2 & -b_3 \\ -b_0 & -b_1 & a_2 & b_3 \\ -b_0 & -b_1 & b_2 & a_3 \end{pmatrix},$$

and

$$\widehat{S}_h^{(4)}(\theta) = \begin{pmatrix} a_0 & -b_1 & -b_2 & b_3 \\ -b_0 & a_1 & b_2 & -b_3 \\ -b_0 & b_1 & a_2 & -b_3 \\ b_0 & -b_1 & -b_2 & a_3 \end{pmatrix}.$$

As before, a different relaxation parameter  $\omega$  could be used for each of the four sweeps. Both of the above schemes offer potential advantages: the CF scheme preserves the symmetry of the hexagonal grid, and the 4C scheme requires less storage. Values of the smoothing factors for these schemes are given in the following section.

**6. Comparison with numerical results.** The canonical model problem for elliptic equations is the Poisson problem. Here we consider

$$(6.1) \quad -\nabla^2 u(x, y) = f(x, y) \quad \text{on } \Omega = [0, 2] \times [0, \sqrt{3}],$$

with periodic boundary conditions in  $x$  and  $y$ . The true solution is specified as  $u(x, y) = \cos(\pi x) \sin(2\pi y/\sqrt{3})$ , and the corresponding forcing  $f$  is computed analytically using (6.1). Unless otherwise specified, this problem is discretized using the second-order discretization (2.2) on a uniform hexagonal grid with mesh size  $h = 1/32$  (i.e., 64 grid points in each of the oblique coordinates) and the restriction operator is full weighting. Coarser grids have mesh sizes successively doubled, with  $h = 1$  on the coarsest grid. We also consider (briefly) a fourth-order discretization, the related modified Helmholtz problem, and spherical geodesic grids below.

For an algorithm consisting of repeated  $V(\nu_1, \nu_2)$  cycles, the observed residual reduction per fine-grid relaxation sweep is measured by the factor

$$\mu_N := \left( \frac{\|\tilde{r}_h\|}{\|\tilde{r}_h\|} \right)^{1/(\nu_1 + \nu_2)},$$

where  $\tilde{r}_h := f_h - L_h \tilde{u}_h$  is the residual before one V-cycle and  $\bar{r}_h$  is the corresponding residual after the cycle, and the norm is defined as  $\|r_h\| := [\sum_i \sum_j (r_{ij}^h)^2 h^2]^{1/2}$ . The

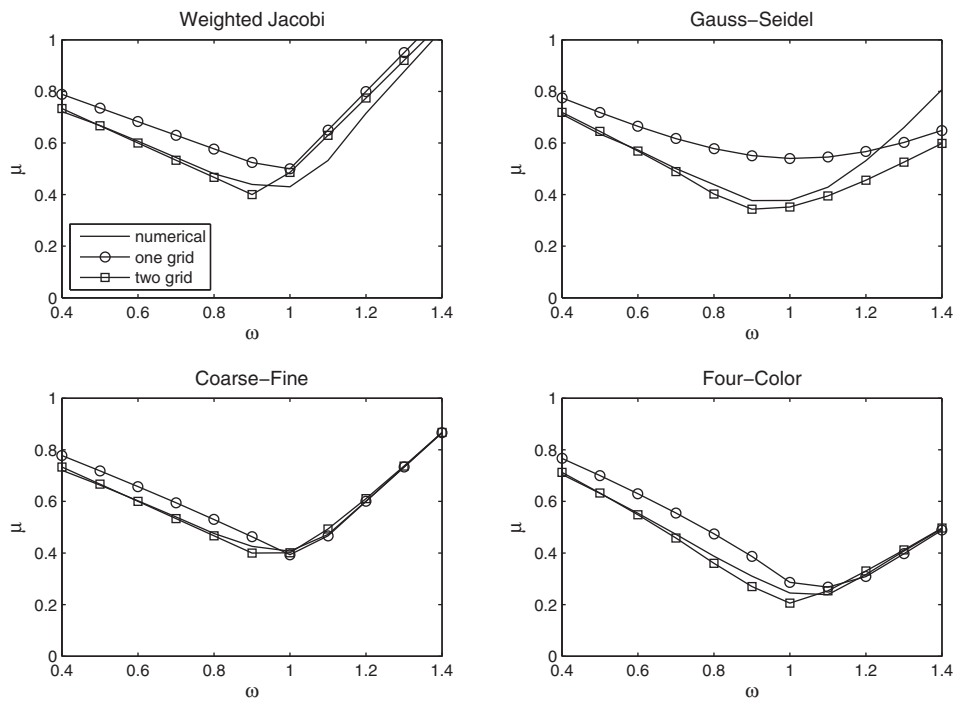


FIG. 6.1. Smoothing factors (one-grid, two-grid, and numerical) as functions of the relaxation parameter  $\omega$  for the Poisson problem using the four relaxation schemes as labeled and  $V(1, 1)$  cycles.

factor  $\mu_N$  should closely approximate the one- and two-grid smoothing factors  $\mu_1$  and  $\mu_2$ ; values reported here are the asymptotic values observed during 10 cycles.

Figure 6.1 shows the performance (analysis and actual) of the four relaxation schemes considered above, using multigrid  $V(1, 1)$  cycles. The curves plot the smoothing factors per sweep ( $\mu_1$ ,  $\mu_2$ , or  $\mu_N$ ) as functions of the relaxation parameter  $\omega$ ; for the CF and 4C schemes the same value of  $\omega$  was used for each partial sweep. In each case the numerical results agree well with the analytical results (especially the two-grid analysis), and the optimal relaxation parameter is close enough to  $\omega = 1$  that using the simpler unweighted relaxation would perform nearly as well. Very similar results are obtained for  $V(1, 2)$  cycles (see Figure 6.2), and the three-grid analysis provides similar estimates for this problem as expected (see Figure 6.3).

The above results were all produced using full weighting as the restriction operator. Using injection instead degrades the performance, as shown in Figure 6.4 for the WJ and GS schemes.<sup>1</sup> Also, using injection with WJ relaxation requires underrelaxation ( $\omega < 1$ ) for optimum performance, which is not required with full weighting. The difference between the analytical and numerical results may be related to the fact that injection (unlike full weighting) does not preserve the integral of the residual it transfers, which means that the right-hand side of the coarse-grid problem (in the periodic case considered here) no longer satisfies the compatibility condition. Indeed, numerical results (not shown) for the corresponding Dirichlet problem—which does not have a compatibility condition—show better agreement with the analysis. Since

<sup>1</sup>Since using injection makes sense only when the residual is smooth, no results are shown for the CF and 4C schemes with injection (in fact, it performs poorly for these schemes).

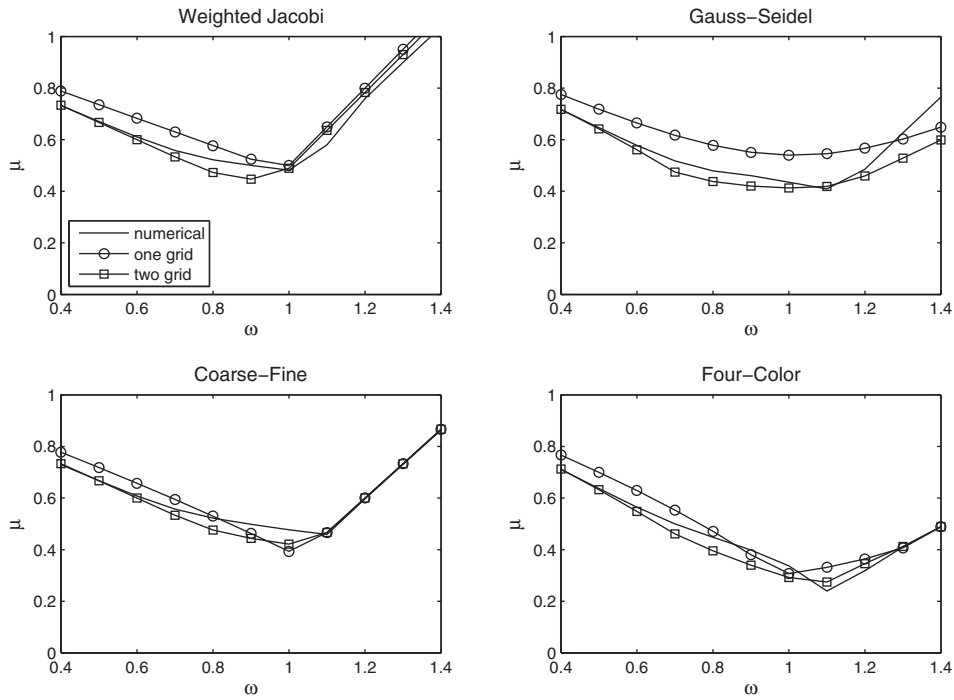


FIG. 6.2. Same as Figure 6.1 except for  $V(1, 2)$  cycles.

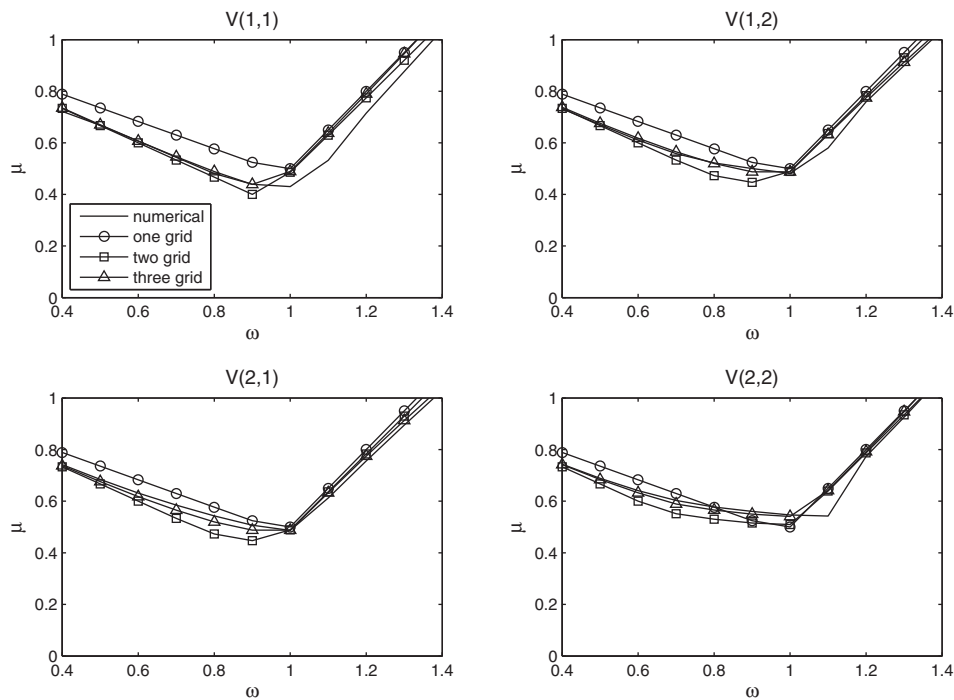


FIG. 6.3. Smoothing factors (one-grid, two-grid, three-grid, and numerical) for weighted Jacobi relaxation and  $V(\nu_1, \nu_2)$  cycles as labeled.

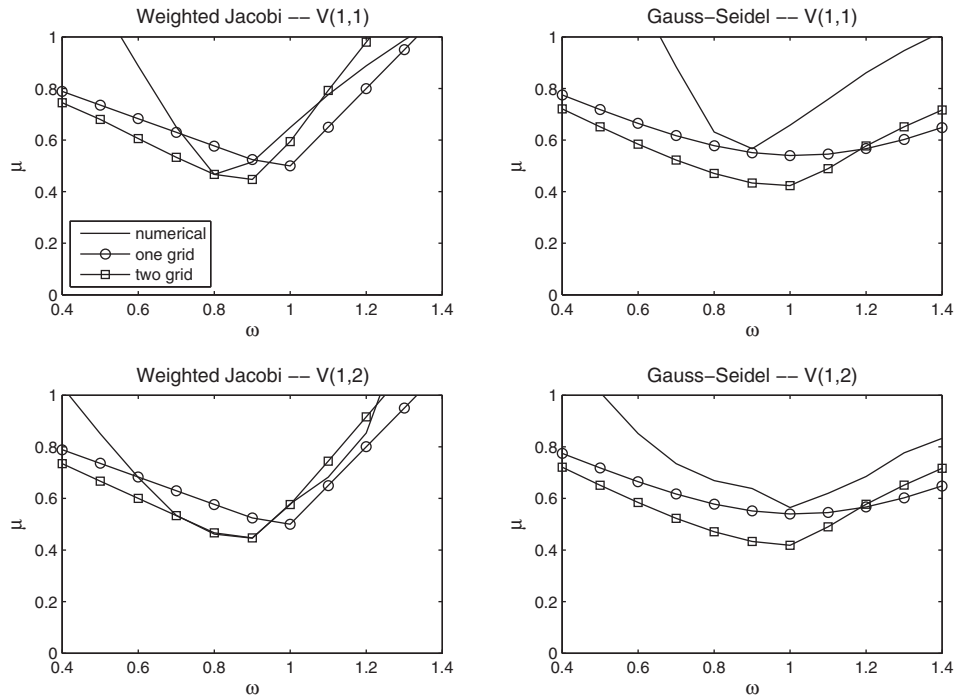


FIG. 6.4. Same as Figures 6.1 and 6.2 except using injection.

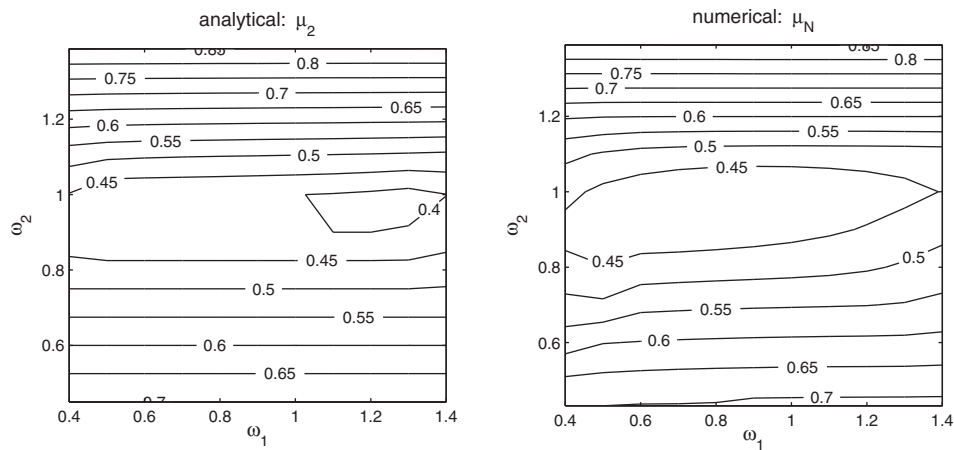


FIG. 6.5. Two-grid smoothing factor  $\mu_2$  and numerical smoothing factor  $\mu_N$  for weighted Jacobi relaxation with coarse-fine ordering as functions of the relaxation parameters  $\omega_1$  and  $\omega_2$  for the coarse and fine sweeps, respectively.

using injection leads to larger smoothing factors than does full weighting (in the cases where it works at all), it will not be considered further here.

The coarse-fine and four-color schemes analyzed in section 5 permit using a different relaxation parameter for each partial sweep. For the coarse-fine scheme the dependence on the two relaxation parameters ( $\omega_1$  and  $\omega_2$  for the coarse and fine sweeps, respectively) is shown in Figure 6.5, which gives the smoothing factors  $\mu_2$

TABLE 6.1

Smoothing factors (per sweep) for the CF scheme with optimal relaxation parameters and corresponding values without weighting.

| Cycles | Factor  | Optimal parameters |            | Smoothing factor |            |
|--------|---------|--------------------|------------|------------------|------------|
|        |         | $\omega_1$         | $\omega_2$ | Optimal          | Unweighted |
| V(1,1) | $\mu_1$ | 1.3810             | 1.0150     | 0.3540           | 0.3937     |
|        | $\mu_2$ | 1.3100             | 0.9690     | 0.3627           | 0.4010     |
|        | $\mu_N$ | 0.8460             | 0.9820     | 0.4032           | 0.4070     |
| V(1,2) | $\mu_1$ | 1.3970             | 1.0170     | 0.3560           | 0.3936     |
|        | $\mu_2$ | 0.4956             | 1.0112     | 0.3483           | 0.4214     |
|        | $\mu_N$ | 0.4100             | 1.0840     | 0.4065           | 0.4772     |

TABLE 6.2

Smoothing factors (per sweep) for the second-order Poisson problem for four (unweighted) relaxation schemes with full weighting.

| Relaxation | Cycles | Analytical |          | Numerical          |                    |                     |
|------------|--------|------------|----------|--------------------|--------------------|---------------------|
|            |        | One-grid   | Two-grid | $h = \frac{1}{32}$ | $h = \frac{1}{64}$ | $h = \frac{1}{128}$ |
| WJ         | V(1,1) | 0.5000     | 0.4859   | 0.4301             | 0.4402             | 0.4431              |
|            | V(1,2) | 0.5000     | 0.4889   | 0.4817             | 0.4842             | 0.4861              |
| GS         | V(1,1) | 0.5399     | 0.3516   | 0.3772             | 0.3848             | 0.3918              |
|            | V(1,2) | 0.5399     | 0.4128   | 0.4348             | 0.4368             | 0.4383              |
| CF         | V(1,1) | 0.3937     | 0.4010   | 0.4070             | 0.4144             | 0.4180              |
|            | V(1,2) | 0.3936     | 0.4214   | 0.4772             | 0.4785             | 0.4790              |
| 4C         | V(1,1) | 0.2865     | 0.2061   | 0.2452             | 0.2519             | 0.2588              |
|            | V(1,2) | 0.3076     | 0.2920   | 0.3373             | 0.3391             | 0.3397              |

and  $\mu_N$  for V(1,1) cycles; the agreement between the analytical and numerical results is good. However, the numerical values summarized in Table 6.1 show there is not a large difference between the smoothing with optimal relaxation parameters and the simpler unweighted scheme ( $\omega_1 = \omega_2 = 1$ ). In view of this result a similar optimization was not explored for the four-color scheme (which already achieves excellent performance without weighting).

Table 6.2 summarizes the smoothing factors (analytical and numerical) for the four relaxation schemes considered here (all unweighted, i.e., with  $\omega = 1$ ). In each case the analysis predicts the actual performance with reasonable accuracy, with the two-grid analysis faring slightly better. All schemes exhibit smoothing factors which are nearly independent of the mesh size. Numerical smoothing factors for V(2,1) cycles (not shown) are close to those for V(1,2) cycles but typically slightly larger. The best performance is achieved by the four-color (4C) scheme and is comparable to the RB scheme on a rectangular grid.

A remarkable feature of the hexagonal grid is that it provides an especially simple fourth-order discretization of the Poisson problem. In the appendix it is shown that the discretization

$$(6.2) \quad \frac{2}{3h^2} \left( 6u_0 - \sum_{i=1}^6 u_i \right) = \frac{3}{4}f_0 + \frac{1}{24} \sum_{i=1}^6 f_i$$

has fourth-order accuracy. This is the hexagonal-grid analogue of the so-called ‘‘Mehrstellen Verfahren’’ discretization [9], but it is markedly simpler: it involves only seven points, and the weights at all surrounding points are the same—both for the solution and the forcing. Furthermore, the operator on the left is identical to that in the second-

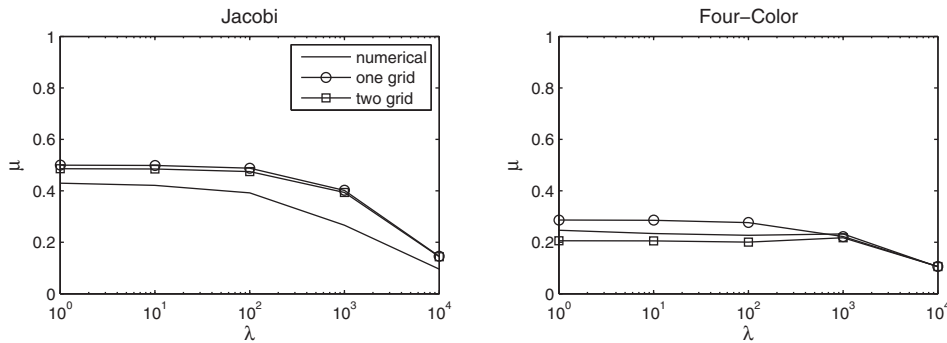


FIG. 6.6. Smoothing factors (one-grid, two-grid, and numerical) as functions of the parameter  $\lambda$  for the modified Helmholtz problem using the (unweighted) Jacobi and four-color schemes with  $V(1, 1)$  cycles.

order discretization (2.2), so only the right-hand side of the second-order discretization needs to be modified to obtain fourth-order accuracy (in the multigrid context this must be done only on the finest grid). The analytical smoothing factors for the two discretizations are identical; numerical smoothing factors for the fourth-order scheme (not shown) match those shown in Table 6.2 for the second-order scheme quite closely.

A slight generalization of the Poisson equation is the modified Helmholtz equation

$$(6.3) \quad \lambda u(x, y) - \nabla^2 u(x, y) = f(x, y),$$

where  $\lambda$  is a positive constant. Using the second-order discretization (2.2) for the Laplacian leads to the discretization

$$\lambda u_0 + \frac{2}{3h^2} \left( 6u_0 - \sum_{i=1}^6 u_i \right) = f_0.$$

The symbol for weighted Jacobi relaxation is

$$\tilde{S}_h^J(\theta, \omega) = (1 - \omega) + \frac{4\omega}{12 + 3h^2\lambda} [\cos(\theta_1) + \cos(\theta_2) + \cos(\theta_1 - \theta_2)],$$

where  $\omega$  is the relaxation parameter. Smoothing factors ( $\mu_1$ ,  $\mu_2$ , and  $\mu_N$ ) for this problem (with  $\omega = 1$ ) are shown in Figure 6.6 as functions of  $\lambda$ , with the numerical results computed for the same domain, grid, and analytical solution as used above. As expected, the convergence improves as  $\lambda$  increases; again, the agreement between the analytical and numerical results is substantial.

The methods examined above can also be incorporated into the full multigrid (FMG) algorithm [1]. This quasi-direct algorithm combines nested iteration with a fixed number of multigrid cycles to solve the problem on each successive grid from coarsest to finest. Properly designed, this should solve the problem to the level of truncation error with work proportional to the number of unknowns on the finest grid. Here we consider the following two algorithms for the Poisson problem, both using the (unweighted) four-color scheme and the same grids used above:

- *FMG2*. uses second-order discretization, one  $V(1, 1)$  cycle per level, and fourth-order initial interpolation;
- *FMG4*. uses fourth-order discretization on currently finest level, two  $V(1, 1)$  cycles per level, and sixth-order initial interpolation.

TABLE 6.3

Results from algorithm FMG2. Here  $\tau_h = f_h - L_h u$  is the truncation error,  $r_h = f_h - L_h \tilde{u}_h$  is the residual,  $\varepsilon_h = u_h - u$  is the discretization error, and  $v_h = u_h - \tilde{u}_h$  is the algebraic error, where  $u, u_h,$  and  $\tilde{u}_h$  denote the continuous, discrete, and approximate discrete solutions, respectively.

| $h$             | $\ \tau_h\ $ | $\ \tau_{2h}\  / \ \tau_h\ $ | $\ r_h\  / \ \tau_h\ $ | $\ \varepsilon_h\ $ | $\ \varepsilon_{2h}\  / \ \varepsilon_h\ $ | $\ v_h\  / \ \varepsilon_h\ $ |
|-----------------|--------------|------------------------------|------------------------|---------------------|--|-------------------------------|
| $\frac{1}{8}$   | 2.56e-01     | 3.88                         | 0.52                   | 1.14e-02            | 4.15                                       | 0.16                          |
| $\frac{1}{16}$  | 6.46e-02     | 3.97                         | 0.80                   | 2.82e-03            | 4.04                                       | 0.21                          |
| $\frac{1}{32}$  | 1.62e-02     | 3.99                         | 0.93                   | 7.03e-04            | 4.01                                       | 0.24                          |
| $\frac{1}{64}$  | 4.05e-03     | 4.00                         | 0.99                   | 1.76e-04            | 4.00                                       | 0.25                          |
| $\frac{1}{128}$ | 1.01e-03     | 4.00                         | 1.04                   | 4.39e-05            | 4.00                                       | 0.25                          |
| $\frac{1}{256}$ | 2.53e-04     | 4.00                         | 1.09                   | 1.10e-05            | 4.00                                       | 0.25                          |

TABLE 6.4

Results from algorithm FMG4 (notation as in Table 6.3).

| $h$             | $\ \tau_h\ $ | $\ \tau_{2h}\  / \ \tau_h\ $ | $\ r_h\  / \ \tau_h\ $ | $\ \varepsilon_h\ $ | $\ \varepsilon_{2h}\  / \ \varepsilon_h\ $ | $\ v_h\  / \ \varepsilon_h\ $ |
|-----------------|--------------|------------------------------|------------------------|---------------------|--|-------------------------------|
| $\frac{1}{8}$   | 3.08e-03     | 15.33                        | 0.16                   | 1.37e-04            | 16.40                                      | 0.06                          |
| $\frac{1}{16}$  | 1.95e-04     | 15.83                        | 0.20                   | 8.51e-06            | 16.10                                      | 0.04                          |
| $\frac{1}{32}$  | 1.22e-05     | 15.96                        | 0.25                   | 5.31e-07            | 16.02                                      | 0.06                          |
| $\frac{1}{64}$  | 7.63e-07     | 15.99                        | 0.28                   | 3.32e-08            | 16.01                                      | 0.06                          |
| $\frac{1}{128}$ | 4.77e-08     | 16.00                        | 0.32                   | 2.07e-09            | 16.00                                      | 0.06                          |
| $\frac{1}{256}$ | 2.98e-09     | 16.03                        | 0.36                   | 1.29e-10            | 16.03                                      | 0.06                          |

Tables 6.3 and 6.4 summarize the results from the algorithms FMG2 and FMG4, respectively. In both cases the truncation error  $\tau_h$  and discretization error  $\varepsilon_h$  decrease with  $h$  at the proper rates, and the problem is solved to or below the level of truncation error, i.e.,  $\|r_h\| \lesssim \|\tau_h\|$  and  $\|v_h\| < \|\varepsilon_h\|$ .

Finally, while our analysis is for uniform hexagonal grids, it also provides useful estimates for spherical geodesic grids, which consist of many quasi-uniform hexagonal cells together with twelve pentagonal cells. Heikes and Randall [4] introduced a multigrid method for the Poisson problem on such grids which uses weighted Jacobi relaxation and injection. As shown in Figure 6.7 (top left panel), the hexagonal-grid analysis accurately predicts the performance of this method, and underrelaxation ( $\omega < 1$ ) is required for best performance. As before, better agreement with analysis (and better performance without weighting) is obtained using full weighting (Figure 6.7 (top right panel)), which on the geodesic grid takes the form [cf. (4.8)]

$$(I_h^{2h} \psi_h)_0 = \frac{A_0(\psi_h)_0 + \frac{1}{2} \sum_{i=1}^n A_i(\psi_h)_i}{A_0 + \frac{1}{2} \sum_{i=1}^n A_i}.$$

Here, the subscripts 0 and  $i$  index the coarse-grid point and the  $n$  surrounding fine-grid points ( $n = 5$  or  $6$ ) and  $A_0$  and  $A_i$  denote the areas of the corresponding fine-grid cells. As suggested by the hexagonal-grid analysis, the CF and 4C schemes perform well on the geodesic grid (Figure 6.7 (bottom two panels)), with the (unweighted) 4C scheme achieving a smoothing factor of about 0.30, again comparable to the RB scheme on a rectangular grid.

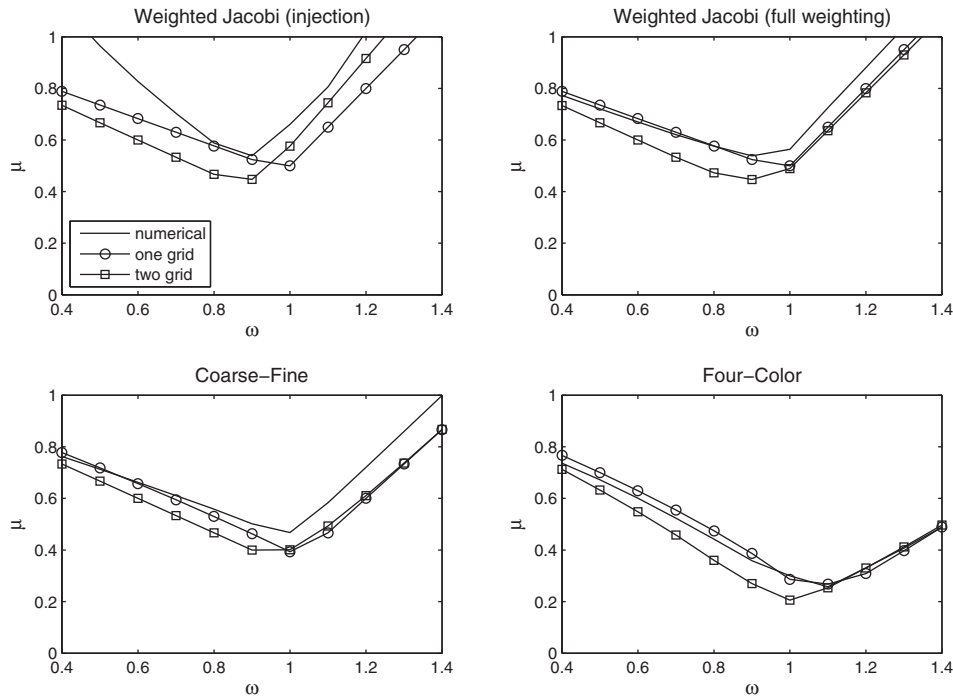


FIG. 6.7. Numerical smoothing factors for the Poisson problem on a spherical geodesic grid with 10,242 cells (five grid levels), compared to the analytical one- and two-grid smoothing factors for a uniform hexagonal grid. The Jacobi results use  $V(1,2)$  cycles; the others use  $V(1,1)$  cycles and full weighting.

**7. Summary and conclusions.** Local Fourier analysis of multigrid methods on hexagonal grids closely parallels that on rectangular grids, provided we express hexagonal grids using oblique coordinates and Fourier modes using a dual basis. Applying this framework to the Poisson problem we have obtained analytical smoothing factors (using one-grid and two-grid analyses) for several relaxation schemes and grid transfers and verified these with numerical calculations. In particular, we find that

- (i) using full weighting, each relaxation scheme tested does not require under- or overrelaxation for nearly optimal performance;
- (ii) Jacobi relaxation (which is parallelizable and preserves the symmetry of the grid) performs nearly as well as Gauss–Seidel relaxation (which is not parallelizable and does not preserve symmetry);
- (iii) Jacobi relaxation with four-color ordering has a smoothing factor of approximately 0.25 for  $V(1,1)$  cycles, making it comparable to Gauss–Seidel relaxation with red-black ordering on the rectangular grid;
- (iv) an especially simple compact fourth-order discretization exists for the Poisson equation on a uniform hexagonal grid;
- (v) second- and fourth-order FMG algorithms on the hexagonal grid solve the Poisson problem to the level of truncation error in work proportional to the number of unknowns;
- (vi) the hexagonal-grid analysis gives quantitatively correct guidance for developing multigrid solvers for spherical geodesic grids.

**Appendix. Fourth-order compact discretization.**

In [6] the existence of a compact fourth-order discretization of the Poisson equation  $-\nabla^2 u = f$  on a uniform hexagonal grid  $\mathbf{G}_h$  is mentioned, but the formula is not given. To derive it, we start with the compact symmetric discretization

$$L_h u_h := \frac{1}{h^2} \begin{bmatrix} -b & -b & 0 \\ -b & a & -b \\ 0 & -b & -b \end{bmatrix} u_h = \begin{bmatrix} d & d & 0 \\ d & c & d \\ 0 & d & d \end{bmatrix} f_h =: I_h f,$$

where  $f_h = f|_{\mathbf{G}_h}$  and the constants  $a, b, c$ , and  $d$  are to be chosen. If the true solution  $u$  is in  $C^6$ , then Taylor expansions yield

$$L_h u = \left( \frac{a - 6b}{h^2} \right) u - \frac{3b}{2} \nabla^2 u + \frac{3b}{32} h^2 \nabla^2 (\nabla^2 u) + O(h^4)$$

for the left-hand side and

$$I_h f = (c + 6d)f + \frac{3d}{2} h^2 \nabla^2 f + O(h^4)$$

for the right-hand side. Using  $f = -\nabla^2 u$  the truncation error is thus

$$\begin{aligned} \tau_h &:= L_h u - I_h f \\ &= \left( \frac{a - 6b}{h^2} \right) u + \left[ \frac{3b}{2} - (c + 6d) \right] \nabla^2 u + \left( \frac{3b}{32} - \frac{3d}{2} \right) h^2 \nabla^2 (\nabla^2 u) + O(h^4). \end{aligned}$$

The discretization will be consistent ( $\tau_h \rightarrow 0$  as  $h \rightarrow 0$ ) if  $a = 6b$  and  $3b/2 = c + 6d$  and fourth-order accurate if  $3b/32 = 3d/2$ . Solving these equations yields  $a = 6b$ ,  $c = 9b/8$ , and  $d = b/16$ . Choosing the normalization  $b = 2/3$  (so that  $L_h u \rightarrow -\nabla^2 u$  and  $I_h f \rightarrow f$  as  $h \rightarrow 0$ ) then gives the discretization

$$\frac{2}{3h^2} \begin{bmatrix} -1 & -1 & 0 \\ -1 & 6 & -1 \\ 0 & -1 & -1 \end{bmatrix} u_h = \frac{1}{24} \begin{bmatrix} 1 & 1 & 0 \\ 1 & 18 & 1 \\ 0 & 1 & 1 \end{bmatrix} f_h,$$

which is (6.2). Since this discretization relies on the fact that  $f = -\nabla^2 u$ , it cannot be extended to the modified Helmholtz equation.

**Acknowledgments.** The authors thank Ross Heikes for helpful comments and copies of his geodesic grid codes, Peter Schultz for helpful discussions, and the anonymous referees for their suggestions.

## REFERENCES

- [1] A. BRANDT, *Multi-level adaptive solutions to boundary-value problems*, Math. Comp., 31 (1977), pp. 333–390.
- [2] M. BREZINA, A. J. CLEARY, R. D. FALGOUT, V. E. HENSON, J. E. JONES, T. A. MANTEUFFEL, S. F. MCCORMICK, AND J. W. RUGE, *Algebraic multigrid based on element interpolation (AMGe)*, SIAM J. Sci. Comput., 22 (2001), pp. 1570–1592.
- [3] W. L. BRIGGS, V. E. HENSON, AND S. F. MCCORMICK, *A Multigrid Tutorial*, 2nd ed., SIAM, Philadelphia, 2000.
- [4] R. HEIKES AND D. A. RANDALL, *Numerical integration of the shallow-water equations on a twisted icosahedral grid. Part I: Basic design and results of tests*, Monthly Wea. Rev., 123 (1995), pp. 1862–1880.

- [5] R. HEIKES AND D. A. RANDALL, *Numerical integration of the shallow-water equations on a twisted icosahedral grid. Part II: A detailed description of the grid and an analysis of numerical accuracy*, Monthly Wea. Rev., 123 (1995), pp. 1881–1887.
- [6] V. L. MAKAROV, S. V. MAKAROV, AND M. N. MOSKAL'KOV, *Spectral properties of the difference Laplacian on a hexagonal mesh and their application*, Differ. Equ., 29 (1993), pp. 959–1118.
- [7] S. NIČKOVIĆ, M. B. GAVRILOV, AND I. A. TOŠIĆ, *Geostrophic adjustment on hexagonal grids*, Monthly Wea. Rev., 130 (2002), pp. 668–683.
- [8] J. W. RUGE AND K. STUÜBEN, *Algebraic multigrid*, in Multigrid Methods, Frontiers Appl. Math. 3, S. F. McCormick, ed., SIAM, Philadelphia, 1987, pp. 73–130.
- [9] S. SCHAFFER, *Higher-order multi-grid methods*, Math. Comp., 43 (1984), pp. 89–115.
- [10] U. TROTTEBERG, C. OOSTERLEE, AND A. SCHÜLLER, *Multigrid*, Academic Press, San Diego, CA, 2001.
- [11] R. WIENANDS AND W. JOPPICH, *Practical Fourier Analysis for Multigrid Methods*, CRC Press, Boca Raton, FL, 2005.
- [12] R. WIENANDS AND C. W. OOSTERLEE, *On three-grid Fourier analysis for multigrid*, SIAM J. Sci. Comput., 23 (2001), pp. 651–671.
- [13] I. YAVNEH AND E. OLVOVSKY, *Multigrid smoothing for symmetric nine-point stencils*, Appl. Math. Comput., 92 (1998), pp. 229–246.